

Towards a model of photon-axion conversion in the host galaxy of GRB 221009A

Sergey Troitsky^{a,b}

^aInstitute for Nuclear Research of the Russian Academy of Sciences,
60th October Anniversary Prospect 7a, Moscow 117312, Russia

^bFaculty of Physics, M.V. Lomonosov Moscow State University,
1-2 Leninskie Gory, Moscow 119991, Russia

E-mail: st@ms2.inr.ac.ru

Abstract. GRB 221009A was the brightest gamma-ray burst ever detected on Earth. In its early afterglow phase, photons with exceptional energies above 10 TeV were observed by LHAASO, and a photon-like air shower above 200 TeV was detected by Carpet-2. Gamma rays of very high energies can hardly reach us from the distant GRB because of pair production on cosmic background radiation. Though final results on the highest-energy photons from this GRB have not been published yet, a number of particle-physics solutions to this problem were discussed in recent months. One of the most popular ones invokes the mixing of photons with axion-like particles (ALPs). Whether this is a viable scenario, depends crucially on the magnetic fields along the line of sight, which are poorly known. Here, we use the results of recent Hubble Space Telescope observations of the host galaxy of GRB 221009A, combined with magnetic-field measurements and simulations for other galaxies, to construct a toy model of the host-galaxy magnetic field and to estimate the rate of the photon-axion conversion there. Thanks, in particular, to the exceptional edge-on orientation of the host galaxy, strong mixing appears to be natural, both for LHAASO and Carpet-2 energy bands, for a wide range of ALP masses $m \lesssim 10^{-5}$ eV and photon couplings $g \gtrsim 10^{-11}$ GeV⁻¹.

Keywords: galactic magnetic fields, ultra high energy photons and neutrinos, axions

ArXiv ePrint: [2307.08313](https://arxiv.org/abs/2307.08313)

Contents

1	Introduction	1
2	Magnetic field of the host galaxy of GRB 221009A	3
2.1	Observational information about the host galaxy	3
2.2	Construction of the toy field model	4
2.2.1	Procedure	4
2.2.2	Planar field of a spiral galaxy: the Milky Way	4
2.2.3	Matching observations of a nearby edge-on disk galaxy: NGC 891	5
2.2.4	From NGC 891 to the host galaxy: scaling	5
3	Photon–ALP conversion probability	7
3.1	Formalism	7
3.2	Unknown unknowns	9
3.3	Results	9
4	Discussion and conclusions	10
4.1	Variations in the field model	10
4.2	From strong mixing in HG to ALP interpretations of GRB 221009A observations	12
4.3	Summary	13
A	Expressions for the field model	14
A.1	Disk field	14
A.2	Toroidal halo field	14
A.3	X-shaped halo field	14
A.4	Total field components	14

1 Introduction

Opacity of the Universe for high-energy gamma rays, caused by e^+e^- pair production on soft background photons [1], is a powerful tool to constrain several exotic particle-physics models or to search for their manifestations, see e.g. [2–4] for reviews. Modification of particle-physics processes may change the standard pattern of pair production, making it possible to observe energetic photons coming from larger distances. One of widely studied examples is the mixing [5] of photons with axions or axion-like particles (ALPs) in the external magnetic field, which may either increase considerably the absorption length of photons [6, 7], or allow for conversion of a part of gamma-ray flux into ALPs, which travel unattenuated and reconvert back to photons close to the observer [8, 9]. For comparison of the two scenarios, see e.g. [10].

With its unique observational appearance, the GRB 221009A gamma-ray burst [11, 12] is suitable for tests of these new-physics hypotheses. Thanks to a relatively nearby, $z \approx 0.151$ [13, 14], location, and to precise pointing of the jet to us, it was the brightest GRB ever observed [15–17]. Similar events are expected to be seen by a terrestrial observer once per $\gtrsim 10^4$ years only [15]. Photons of exceptionally high energies associated with the burst have been observed by Fermi LAT up to 99 GeV, and possibly even 400 GeV [18–22], and LHAASO WCDA, ~ 0.3 TeV to ~ 5 TeV [23]. Strong interest was attracted by initial claims of events

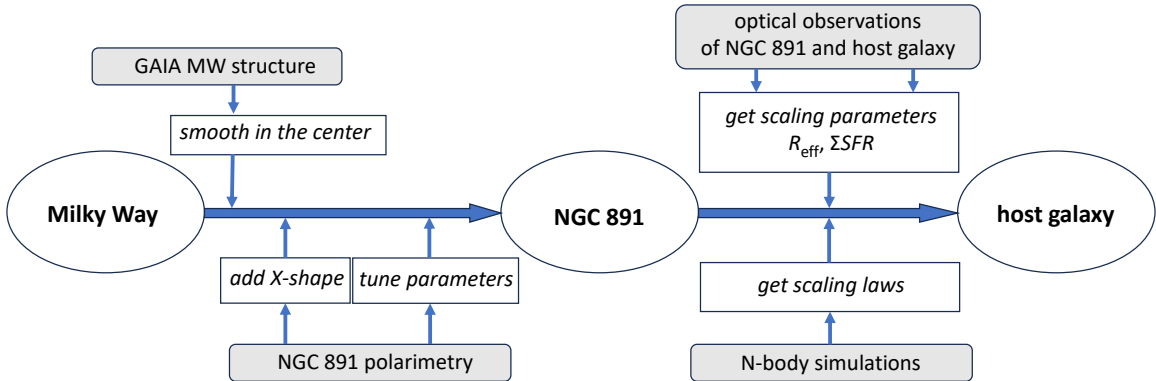


Figure 1. Construction of the toy model of the magnetic field in the host galaxy of GRB 221009A: a schematic view of the procedure. See the text for details.

with energies ≈ 18 TeV by LHAASO KM2A [24] and ≈ 251 TeV by Carpet-2 [25]. For photons of these energies, one expects suppression of the flux so strong that they could hardly reach the Earth from $z \approx 0.151$ unless some anomalous new-physics effects affected the propagation. Both LHAASO KM2A and Carpet-2 have not yet published details of their observations.

Preliminary KM2A results were mentioned in the talk [26]. The energy of the primary particle for each event is determined in a probabilistic way because of inevitable fluctuations in the shower development. As a result, the estimate of the energy of each particular primary photon depends on the assumed energy spectrum, that is of other photons from the same source. The difference between energies reconstructed under different spectral assumptions contributes to systematic uncertainty, because at the highest energies we are interested here, low statistics does not allow to robustly prefer one of the spectral models. For the standard log-parabola assumption, the energy of the highest event associated by LHAASO with GRB 221009A was estimated in [26] as $E = 17.8_{-5.1}^{+7.4}$ TeV, consistent with the initial 18 TeV estimate. If the assumed spectrum is steeper, the most probable energy, within the uncertainties for a particular event, is lower. Other assumptions give $E = 12.2_{-2.4}^{+3.5}$ TeV and $E = 12.5_{-2.4}^{+3.2}$ TeV for the same event [26]. We consider both $E = 18$ TeV and $E = 13$ TeV in the present work. We will see that this uncertainty does not affect significantly the conclusions of our study, changing the range of ALP parameters, for which mixing in the host galaxy is strong, only slightly. Note that this uncertainty is important for interpretation of the observations because of strong energy dependence of the gamma-ray absorption. Implications of these uncertainties for the interpretation may be addressed with full information on the observed spectra, when it is published.

Despite uncertainties, many theoretical publications on the subject address ALP-related [27–36], as well as other [37–46] new-physics explanations of these anomalies.

Quantitative estimates of the photon-ALP conversion probabilities, necessary in particular to assess the viability of the corresponding explanation of the anomalous transparency of the Universe for high-energy photons, require knowledge of cosmic magnetic fields along the line of sight. The lack of knowledge of the fields may result in tremendous systematic uncertainties in astrophysical constraints on ALP-photon mixing [47, 48]. For the energies of photons relevant to the GRB 221009A observations by LHAASO KM2A and Carpet-2, significant changes to the standard photon propagation may happen because of magnetic fields in the GRB host galaxy and in the Milky Way. Even for our Galaxy, the magnetic field is

known with large uncertainties, see e.g. [49–52], and one should rely on purely theoretical models for the distant host galaxy of GRB 221009A.

Soon after the observations by [24] and [25], it has been shown that both LHAASO and Carpet-2 events could be explained by ALP-photon mixing, provided this mixing is close to maximal in the host galaxy [28]. The required ALP parameters are in tension with some model-dependent astrophysical limits, but satisfy constraints from helioscope searches and from stellar evolution, see Sec. 4.2. The assumption of the maximal mixing was reasonably criticized as “wishful thinking” by [30], because nothing was known about the host galaxy for that moment. Assuming that the field in the host galaxy is described by one of the models developed for the Milky Way, and varying the orientation of the host galaxy with respect to the line of sight, [34] claimed that the maximal mixing is not possible for photons of both 18 TeV and 251 TeV simultaneously.

Newer observations of GRB 221009A by the Hubble Space Telescope (HST) [53] brought important information about the host galaxy, and the purpose of the present work is to improve the model of the photon-ALP conversion there by making use of these results. Despite relatively short exposure, Galactic absorption and contamination by the GRB afterglow, these observations severely constrain the conversion model through the galaxy’s geometry, the star formation rate, and the position of the GRB in the host galaxy. We will show that this information has a drastic impact on the conclusions about the maximal mixing, making them opposite to those of Ref. [34], which did not use any observational constraints about the host galaxy. The maximal mixing is possible for both energies for a certain range of parameters. We however do not address the question whether it can simultaneously explain both LHAASO and Carpet-2 events.

In Sec. 2, we construct a toy model of the magnetic field in the host galaxy of GRB 221009A. We start with summarizing relevant observational information in Sec. 2.1 and use it to build the model in Sec. 2.2, with the help of published observations and simulations of other disk galaxies, including our Milky Way. In Sec. 3, we use this model to estimate the photon-ALP conversion rates in the host galaxy, putting the photon source to the GRB. The results are summarized and discussed in Sec. 4. Explicit expressions for the field model of the host galaxy are summarized in Appendix A for reference.

2 Magnetic field of the host galaxy of GRB 221009A

2.1 Observational information about the host galaxy

The distance to GRB 221009A was determined by spectroscopic observations of the afterglow [13, 54] and of the host galaxy (HG) [14, 55]. The redshift is $z = 0.151$; assuming the standard cosmology with $\Omega_M = 0.3$, $\Omega_\Lambda = 0.7$ and $h = 0.7$, the luminosity distance is $d_L \approx 718$ Mpc and the angular separation of $1''$ corresponds to the projected linear size of 2.63 kpc.

HST observations reveal interesting geometry of HG. Ref. [53] presents parameters of the fit to its image with the Sérsic profile, effective half-light radius $R_e = (2.45 \pm 0.20)$ kpc, Sérsic index of 1.71 ± 0.18 and the ratio of half-axes $b/a = 0.22 \pm 0.01$. This geometry is remarkable because it corresponds to a rare edge-on orientation of this disk galaxy. We compare it with a nearby (8.4 Mpc) edge-on spiral NGC 891, for which $b/a \approx 0.24$ [56], and the disk plane is inclined to the line of sight by less than 1° [57]. In what follows, we assume that HG, having even smaller b/a , is seen precisely in the disk plane.

Further, HST images [53] allow one to determine the projected position of GRB 221009A in HG. The projected distance from the galaxy center to the GRB is ≈ 0.65 kpc, with the

component parallel to the disk plane of ≈ 0.48 kpc, and the distance to the middle plane of HG of ≈ 0.44 kpc. The position of the GRB along the line of sight clearly remains unknown, see Sec. 3.2.

According to [53], HG is a typical star-forming galaxy for its redshift, as determined by comparison with other starburst galaxies in general [58] and host galaxies of long GRBs in particular [59] observed by HST. The HG stellar mass M_\star is modest, estimated as $\log_{10}(M_\star/M_\odot) = 9.00^{+0.23}_{-0.47}$ [53].

2.2 Construction of the toy field model

Further observations with longer exposures, after the GRB 221009A afterglow fades, would bring more information about HG; however, given the distance, there is no hope to obtain direct observational constraints on the magnetic field in the galaxy. First observations, already available, give sufficient information to construct a toy field model which can be used to estimate the probability of the photon-ALP conversion.

2.2.1 Procedure

The general approach to construct a model of the HG magnetic field, which we follow in detail below, is illustrated by a scheme in Fig. 1. We start with a model of the magnetic field of the Milky Way, which is based on Faraday rotation measurements of numerous radio sources. This model represents well the magnetic field in the spiral arms, but is not reliable for the central part of the Milky Way. We smooth it close to the center, where the Milky-Way spiral structure is not present. Then, we compare it with magnetic-field measurements in NGC 891, a nearby spiral galaxy which has, like HG, higher star formation rate than the Milky Way, and is seen edge-on. We add halo field and tune parameters of the model to reproduce observational data for this galaxy. Finally, we make use of the scaling of the field model with the effective radius R_e of the galaxy and with the surface density of the star formation rate, ΣSFR , known for both NGC 891 and HG. The scaling relations we use are verified on the set of magnetized disk galaxies obtained in the Auriga simulations.

2.2.2 Planar field of a spiral galaxy: the Milky Way

Various empirical models of the large-scale Milky-Way magnetic field differ in details but share a general spiral-arm geometry, which is expected to be representative also for fields of other disk galaxies, for a review see e.g. [60]. Our starting point is the model by [61]. Like other similar models [49, 62], it is not intended to describe correctly the field in the central part of the Galaxy. Indeed, on one hand, the models are heavily based on observations of the Faraday rotation of extragalactic sources, scarce in the directions close to the Galactic Center. On the other, the models were originally developed for studies of deflections of extragalactic charged cosmic-ray particles, arriving isotropically, so that only a small fraction of their flux goes through the central part of the Galaxy. One therefore needs to extend the spiral-arm field model to the central regions of the disk.

Recent analyses of the GAIA data, e.g. [63], demonstrate that the spiral arms of the Milky Way are traced down to central distances of ~ 2.5 kpc. We smooth the field model of [61] at these distances, switching off the spiral-arm structure in such a way that the disk field reaches a value independent of the polar angle in the disk, and then vanishes at the center. Explicit formulae are given in Appendix A.1. Note that this approach is more realistic, compared to simply setting the field to zero in a certain central region, like e.g. in the model

of [49]. However, not being based on observations, this exact functional form of the field in the central region is not guaranteed.

2.2.3 Matching observations of a nearby edge-on disk galaxy: NGC 891

Compared to a typical host galaxy of a GRB, our Milky Way is larger and has lower star-formation rate, cf. [64]. In addition, Faraday rotation measurements performed from inside the Galaxy are less sensitive to the magnetic-field component perpendicular to the disk, while this component is important for photon-ALP conversion, given the HG orientation. Indeed, the Faraday rotation is determined by the field component along the line of sight, but the ALP conversion probability is governed by the perpendicular one, see Sec. 3. With this motivation, we choose to modify our field model to match observations of a nearby edge-on disk galaxy, NGC 891, already mentioned above.

NGC 891 is well studied thanks to its proximity. Despite being considered as a “Milky-Way twin” [65], NGC 891 is more compact [56] and has the star formation rate about twice higher [66–68], making its properties more similar to those expected for HG.

The magnetic field of NGC 891 was being studied for a long time by different methods [57, 69–73]. It was found that, in addition to the plane-parallel field, X-shaped halo field is prominent. Note that stacked observations of halos of various galaxies suggest that the presence of this field component is general [74]. At the same time, the halo field in the model of [61] is purely toroidal, see Appendix A.2. We introduce the additional X-shape component to the field model. We use Model C of [75]; explicit expressions for the field components are given in Appendix A.3.

The new component is added with an unknown coefficient, and in addition one expects that both the geometrical radial scale and the disk field normalization are different in NGC 891 with respect to the Milky Way. We therefore fit these three parameters to match observations. To achieve this, we make use of published measurements of the reconstructed magnetic field along the central line of NGC 891 by [72] and [57], which are in a remarkably good agreement with each other, see Fig. 2. We average the model field over the polar angle in the disk plane because the orientation and structure of spiral arms is not known. We account for the difference between the regular field B , provided by our model, and the total equipartition field B_{tot} , given in Refs. [57, 72], following approximate relations given in Ref. [60], $B \sim \sqrt{3/2}B_{\perp} \sim 0.3\sqrt{3/2}B_{\text{tot}}$. Note that the turbulent component of the field is marginally relevant for the ALP-photon conversion in the galaxy, see Sec. 4.1. Because of the polar-angle averaging, the model line is left-right symmetric while the data points are not, reflecting the actual spiral structure. The variations in the choice of spiral-arm orientation give additional uncertainty of 14% (one standard deviation); with this uncertainty added in quadrature to the statistical error bars of individual data points, the goodness of the fit is 96.4% ($\chi^2 \approx 5.2$ for 12 degrees of freedom). Given rich results of the field measurements, it would be possible to construct a much more precise model for NGC 891, but for our purposes the present toy model is sufficient: we plan to adopt it for HG, for which there are no chance to observe the spiral-arm structure.

2.2.4 From NGC 891 to the host galaxy: scaling

At this final step in the field model construction, we scale the field strength and geometrical parameters to account for the differences between NGC 891 and HG.

Magnetic field strength increases with the star formation rate (SFR), which can be understood with equipartition arguments, e.g. by [76], suggesting that the total field scales as

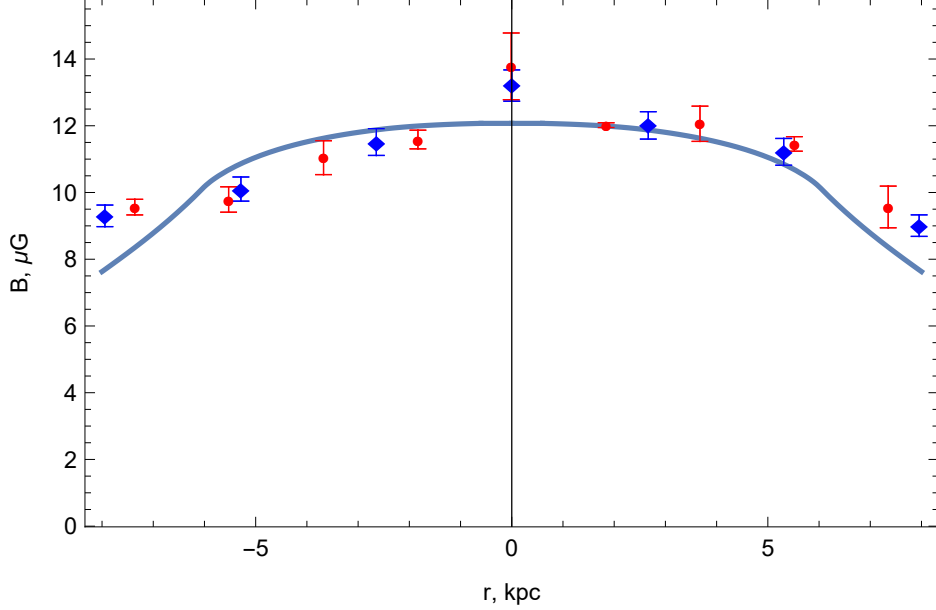


Figure 2. The profile of the total magnetic field along the central line of NGC 891: our model (line) versus observations by [72] (red circles) and [57] (blue diamonds).

$B \propto (\text{SFR})^{0.4}$. Other studies established a more pronounced scaling of B with the SFR surface density, ΣSFR . The proportionality $B \propto (\Sigma\text{SFR})^{1/3}$ [77] was expected for nearby galaxies; see [78] for a detailed recent discussion and further references. Simple equipartition arguments, see e.g. [79], suggest that $B \propto (\Sigma\text{SFR}/v)^{1/2}$, where v is the escape velocity of cosmic rays. The exponent of $1/3$ is reproduced under the assumption of $v \propto (\Sigma\text{SFR})^{1/3}$ which is realistic. It is in agreement with observed values of 0.33 ± 0.3 [80] or 0.31 ± 0.06 [81]. However, the observations of the magnetic fields are indirect, and the equipartition assumption may be violated in star-forming galaxies [82], so we test this scaling with the results of detailed cosmological simulations which include the magnetic fields. Figure 3 presents the relation between $M_\star/R_e^2 \propto \Sigma\text{SFR}$, where M_\star is the total stellar mass and R_e is the effective radius, and the central magnetic field B_c for 30 disk galaxies from the *Auriga* simulations [83, 84]. They follow the scaling relation $B_c \propto (M_\star/R_e^2)^{0.44 \pm 0.12}$, with the exponent slightly larger than $1/3$. In what follows, we adopt the scaling $B \propto (\Sigma\text{SFR})^{0.4}$ and note that the effect of the changes in the exponent on our results is negligible. We use this rule to scale the field strengths of all three components of our model from NGC 891 to HG. For the former, we use the value of $\Sigma\text{SFR} \approx 3.13 \times 10^{-3} M_\odot/\text{kpc}^2/\text{yr}$ [68]. For HG, we use the fact that it is a typical star-forming galaxy for its redshift [53] and invoke the relation between M_\star and SFR from [85], making use of Eqs. (15), (12) and Table 2 of that reference. Then we estimate $\Sigma\text{SFR} \sim \text{SFR}/(2\pi R_e^2)$. Here, $1/2$ comes from the fact that R_e is the half-light radius. For $z = 0.151$ and $M_\star = 10^9 M_\odot$, we obtain $\Sigma\text{SFR} \approx 8.5 \times 10^{-3} M_\odot/\text{kpc}^2/\text{yr}$.

Additionally, we need to change all linear scales, listed in Table 1, in the model to reflect the difference in the galaxy sizes. It is natural to use R_e as the scale parameter. We tested with the *Auriga* galaxies that the linear scaling is reasonable, though with a large scatter: the scale of the magnetic field decrease, $r_{0,\text{inner}}^B$, determined from simulations, is proportional to $R_e^{0.88 \pm 0.35}$. We use $R_e = 5$ kpc for NGC 891, consistent with observations by [65] ($R_e \approx 4.9$ kpc) and by [86] (3.93 kpc $< R_e < 5.80$ kpc). For HG, we use $R_e = 2.45$ kpc

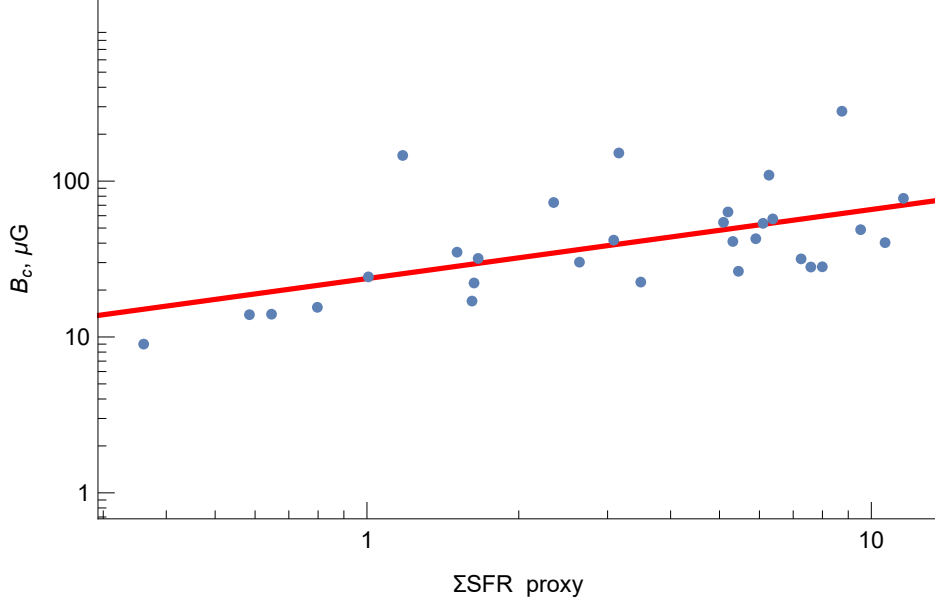


Figure 3. Correlation between specific star formation rate ΣSFR and central magnetic field B_c in *Auriga* simulated galaxies [83, 84]. The proxy for ΣSFR is M_\star/R_e^2 , in units of $10^{10} M_\odot/\text{kpc}^2$. The red line represents the best power-law fit $B_c \propto (\Sigma\text{SFR})^{0.44}$.

determined by [53].

This rescaling finalizes the construction of the toy model of the HG magnetic field. Explicit expressions for the field components and values of parameters for HG are summarized in Appendix A for reference.

Figure 4 illustrates the magnetic field components relevant to the photon-ALP conversion discussed in the next section.

3 Photon–ALP conversion probability

3.1 Formalism

The mixing of photons with light pseudoscalar particles in the external magnetic field underwent extensive theoretical studies since the original works [5, 87], for reviews in the astrophysical context see e.g. [2, 3]. A general ALP has two parameters, mass m and photon coupling g (we follow the notations of [47]). In particle-physics units $\hbar = c = 1$, both m and $1/g$ have the dimension of energy E . The easiest and numerically fast way to estimate the probability of conversion of a photon to an ALP is to introduce the 3×3 density matrix ρ and to find its evolution with the line-of-sight coordinate y described by the equation

$$i \frac{d\rho(y)}{dy} = [\rho(y), \mathcal{M}(E, y)], \quad (3.1)$$

where

$$\mathcal{M} = \frac{1}{2} \begin{pmatrix} \Delta_1 & 0 & igB_1 \\ 0 & \Delta_2 & igB_2 \\ igB_1 & igB_2 & m^2/E \end{pmatrix}, \quad (3.2)$$

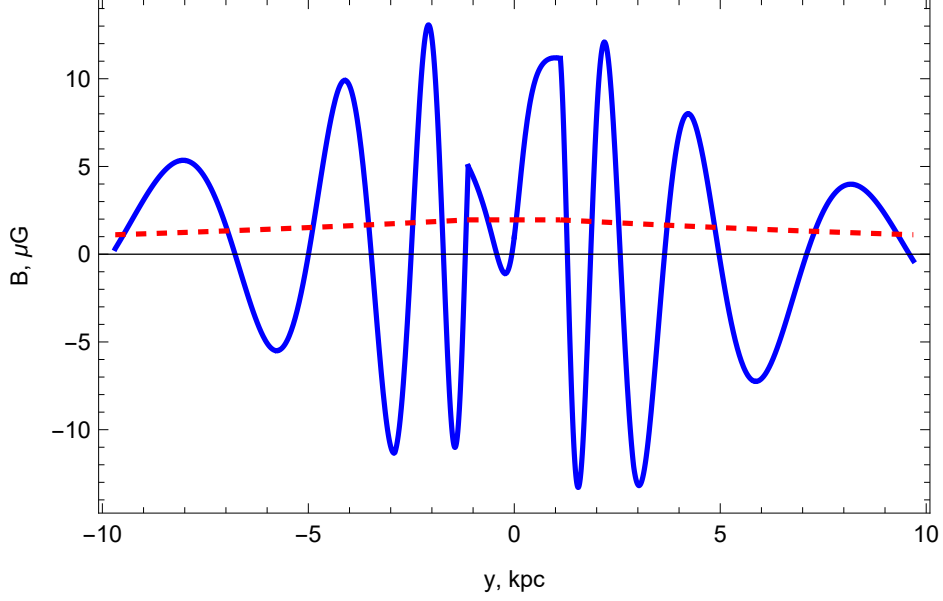


Figure 4. Model HG magnetic field components perpendicular to the line of sight from the Earth to the GRB, as a function of the coordinate y along this line. $\theta_0 = 80^\circ$; $y = 0$ corresponds to the middle line of the galaxy. The blue full line represents the component in the disk plane, the red dashed line is the component perpendicular to the disk.

$B_{1,2}(y)$ are two components of the magnetic field perpendicular to the line of sight, and $\Delta_{1,2}$ are the elements describing photon dispersion. A convenient expression for $\Delta_{1,2}$ reads (see e.g. [9, 88, 89]),

$$\Delta_{1,2} \approx \left(8.0 + 1.43 \left(B_{1,2}^2 + \frac{4}{7} B_{2,1}^2 \right) \right) \times 10^{-8} \text{ pc}^{-1} \frac{E}{\text{TeV}}. \quad (3.3)$$

Here, the first, constant, term in parentheses is due to the interaction with CMB photons [88], while the second one, proportional to B^2 , comes from the QED vacuum polarization [90, 91]. The effect of $\Delta_{1,2}$ grows with energy but, even for $E = 251$ TeV, remains small provided

$$1.3 \left(\frac{g}{10^{-11} \text{ GeV}^{-1}} \right)^{-1} < \frac{B}{\mu\text{G}} < 4.2 \frac{g}{10^{-11} \text{ GeV}^{-1}}. \quad (3.4)$$

Thanks to the exceptional orientation of both HG and the Milky Way, the line of sight crosses several spiral arms, and B changes considerably along it. As a result, the conditions (3.4) are satisfied, for a range of g , at least for a fraction of the line of sight, sufficient for the photon-ALP conversion. In the numerical calculations, $\Delta_{1,2}$ were included. In the expression (3.3), we kept only the terms which are not negligible for the parameter ranges we are interested in here. Complete expressions for other terms, which include the plasma-related photon dispersion and terms in the vacuum dispersion suppressed by $\kappa = (E/m_e)(B/B_{\text{cr}})$, where m_e is the electron mass and $B_{\text{cr}} = m_e^2/e \approx 4 \times 10^{13}$ G, can be found e.g. in [9]. The plasma term may be neglected provided the electron density n_e satisfies

$$n_e \ll 10^5 \text{ cm}^{-3} \frac{B}{\mu\text{G}} \frac{g}{10^{-11} \text{ GeV}^{-1}} \frac{E}{\text{TeV}}, \quad (3.5)$$

which is safely fulfilled even in the star-forming regions. Smallness of higher-order terms in κ is guaranteed by the condition

$$\kappa \approx 1.8 \times 10^{-14} \frac{B}{\mu\text{G}} \frac{E}{\text{TeV}} \ll 1. \quad (3.6)$$

The assumption that the emitted photons are not polarized is equivalent to the initial condition

$$\rho(y_0) = \text{diag}(1/2, 1/2, 0). \quad (3.7)$$

Then, the probability to observe an ALP at a distance y from the source is given by the $\rho_{33}(y)$ component of the solution $\rho(y)$ to Eq. (3.1) with the boundary condition (3.7).

3.2 Unknown unknowns

For a given energy and fixed ALP parameters, the conversion probability is determined by the evolution of $B_{1,2}$ along the line of sight. We will use the toy model developed in Sec. 2.2 to estimate this probability for HG. However, even if the model were precise, it would represent an unrealistic task to determine two important parameters. One is the orientation of the spiral arms in the disk plane, mentioned already in Sec. 2.2.3, parameterized by the zero point θ_0 of the polar angle θ in expressions of Appendix A. Another is the deprojected location of the GRB site in HG, which determines the zero point y_0 of the coordinate y along the line of sight, where the condition (3.7) should be applied.

To tackle this issue, we consider a variety of possible values for the both parameters and perform calculations for different assumptions. *A priori*, all orientations of spiral arms have equal probabilities, while the position of the GRB along the line of sight is expected to follow the stellar distribution. To estimate the latter, we use parameters of the Sérsic profile of HG reported by [53] and reconstruct the deprojected luminosity distribution following [92, 93].

The calculations are performed as follows. For each pair of (m, g) on a logarithmic grid, $-9 \leq \log_{10}(m/\text{eV}) \leq -5$, and $-12 \leq \log_{10}(g/\text{GeV}^{-1}) \leq -9.5$, with the step of 0.1 in both cases, and for each of the two energies, 18 TeV and 251 TeV, we generate 100 pairs of random numbers (θ_0, y_0) , where the uniformly distributed $0 \leq \theta_0 < 2\pi$ is the zero point of θ with respect to the direction perpendicular to the line of sight, and y_0 is the GRB location along the line of sight, distributed following the deprojected luminosity distribution in HG. Fixing the field geometry by θ_0 and the GRB location by y_0 , we calculate the probability for a photon to convert to ALP in HG for this case.

3.3 Results

For each point in the parameter space, we thus obtain a distribution of the probabilities for an energetic photon emitted from GRB 221009A to convert to an ALP in HG, reflecting the freedom in θ_0 and y_0 . To formulate the results, we select the parameters for which the probability exceeds 32% (maximal mixing) or 10% (strong mixing) for at least 68% of realizations of (θ_0, y_0) .

The results are presented in Fig. 5. For a wide range of ALP parameters m and g , strong mixing in HG is possible both for $E = 18$ TeV and $E = 251$ TeV. The same is true for somewhat lower energies, like $E = 13$ TeV, obtained for the highest-energy LHAASO event under different assumptions. As it is expected from simple estimates, e.g. [9], efficient conversion at higher energy, 251 TeV, is possible for higher ALP masses; we note that the

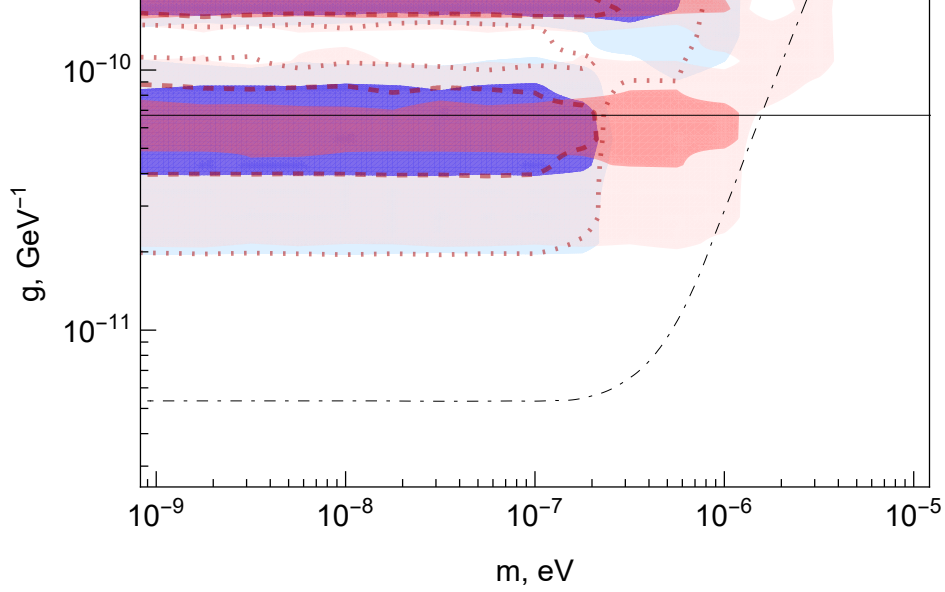


Figure 5. The ALP parameter space: mass m and photon coupling g . For parameters in the shaded regions, maximal (conversion probability $> 32\%$, dark shading) or strong (conversion probability $> 10\%$, light shading) photon-ALP mixing in the host galaxy occurs for $> 68\%$ of geometry realisations, see the text. Blue shading corresponds to $E = 18$ TeV, pink shadings – to $E = 251$ TeV. In the darkest regions, they overlap and the maximal mixing happens for both energies. Dashed and dotted lines delimit the regions of maximal and strong mixing, respectively, assuming $E = 13$ TeV. The full line represents the upper limit on g from the search of solar ALPs in the CAST experiment [94], coinciding with the limit from the evolution of horizontal-branch stars in globular clusters [95]. The dash-dotted line represents the upper limit on g from magnetic white dwarf polarization [96], the strongest of astrophysical limits which assume a particular magnetic-field configuration in the source. Purely laboratory experiments give limits too weak to be shown in this plot, see [48] for their compilation.

conversion probability for 18-TeV photons there is lower but not negligible. The complicated structure of the plot reflects the fact that for strong mixing, for fixed distance of the source and for a given magnetic field, the conversion probability is an oscillating function of the ALP parameters. Additional complications arise from the structure of the spiral-arm field and the procedure of sampling the “unknown unknowns”.

Figure 6 presents the energy dependence of the photon survival probability at the exit from HG for a particular realization, $\theta_0 = 0$ and $\gamma = 80^\circ$, of the magnetic field. It demonstrates that, indeed, the maximal mixing is possible for the energy range which includes both 13 TeV and 251 TeV. At higher energies, dispersion effects suppress the mixing.

4 Discussion and conclusions

4.1 Variations in the field model

We have demonstrated that, within the particular toy model of the HG magnetic field we constructed, strong photon-ALP mixing is possible in HG for photon energies corresponding to observations of GRB 221009A by both LHAASO KM2A and Carpet-2. While the field model reflects the best up-to-date knowledge about HG, variations in the field strength and

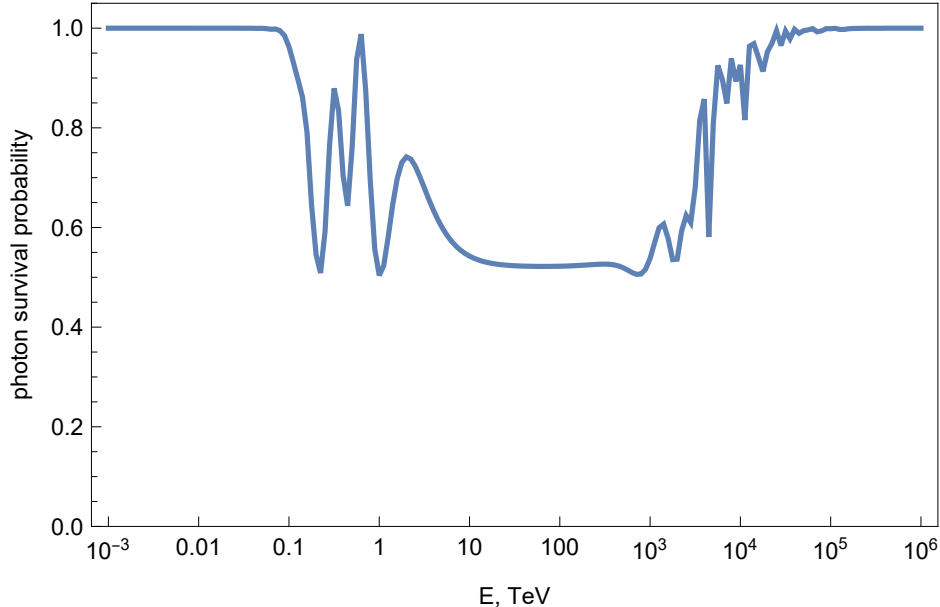


Figure 6. The energy dependence of the photon survival probability at the exit of HG, assuming $m = 10^{-7}$ eV, $g = 6 \times 10^{-11}$ GeV $^{-1}$, $y_0 = 0$, $\theta_0 = 80^\circ$. Absorption in HG is neglected.

configuration may change the conversion probabilities. These variations may come from several sources.

Firstly, our starting point was a model of the Milky-Way magnetic field, which is also not firmly known. Particular models give different results, especially considering the field outside the disk, but also regarding the disk field normalization. However, these differences are not relevant for our study because we take only the shape of the disk field from this model, and subsequently change both the field strength and geometric scales as described in Sec. 2.2.3, 2.2.4. The halo field is also added independently, Sec. 2.2.3. Therefore, our field model essentially inherits only the overall spiral-arm structure from the original Milky-Way field, which is based on the Galaxy structure and does not vary between models. This makes the result insensitive to the choice of the original model, so we safely use the model of [61], for which simple analytical expressions are available, see Appendix A.1.

Secondly, we discuss here only the regular large-scale magnetic fields, while the total field strength in galaxies includes non-negligible turbulent component. It is especially strong in regions of intense star formation [97], which are plausible sites of GRBs [59]. However, the fields with coherence lengths $\lesssim 100$ pc, which is a typical size of a star-forming region, have very little effect on the ALP conversion: the turbulent field is of a similar order as the regular one, or a factor of a few stronger, but its relatively rapid change does not allow the conversion to build up coherently. This results in a subleading correction to the total conversion probability, as can be seen from e.g. [9], and justifies the ignorance of the turbulent galactic field in this and other studies. As it is demonstrated e.g. in [98], the turbulent field becomes important for the shape of the spectrum at energies between low and strong mixing. For a detailed quantitative calculation of the effects of the ALP conversion on the observed photon spectra, the turbulent fields may be taken into account, provided their parameters are known robustly. However, they could hardly affect the answer to the main question of the present paper, whether or not the strong mixing in HG is possible.

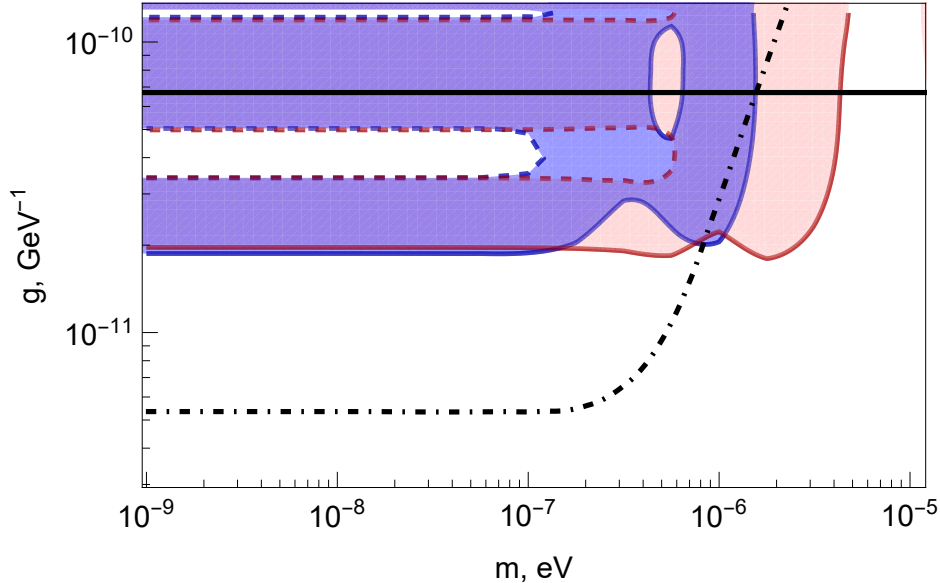


Figure 7. ALP parameters (mass m and photon coupling g) for which strong mixing happens in the Milky Way (regions limited by dashed lines, direction to GRB 221009A, field model [61]) and in HG (regions limited by full lines, the field configuration with $y_0 = 0$ and $\theta_0 = 80^\circ$). For parameters in the shaded regions (blue for $E = 18$ TeV, pink for $E = 251$ TeV, violet for both energies), the mixing is strong in both galaxies. Other notations are the same as in Fig. 5.

4.2 From strong mixing in HG to ALP interpretations of GRB 221009A observations

Here, we estimate the ALP-photon mixing in HG only. To assess whether high-energy photons from GRB 221009A may indeed be related to ALPs, one needs (i) to calculate the probability of the mixing along the entire way from the source to the observer, and (ii) to compare the predicted photon spectrum, taking the potential impact of ALPs into account, with observations. The point (i) was addressed in various works, e.g. [27–30] etc. Mixing in the intergalactic space is expected to be small, and the resulting probability is determined by the conversion in HG, calculated here, and reconversion in the Milky Way. Note that, because of the low Galactic latitude of GRB 221009A, $b \approx 4^\circ$, the line of sight passes through the disk of our Galaxy as well, providing conditions for strong conversion. Figure 7 demonstrates that the strong conversion in both galaxies is expected for large regions of the parameter space.

However, the point (ii) requires more detailed information about the GRB flux and spectrum at highest energies. Presently, this information is unavailable since the GRB 221009A flux from Carpet-2 has not been published yet, nor a widely accepted model of the GRB emission above 10 TeV exists, which would be necessary to estimate the intrinsic spectrum, and hence the amount of absorption. Therefore, we focus here only on one important element of the scenario and postpone a detailed quantitative interpretation of the observations to future work. It remains to be understood whether the ALP mechanism is necessary to explain the observed gamma-ray spectra, and whether the strong mixing at both LHAASO and Carpet-2 energies is required. If interpretation of the spectra will not require nonstandard physics, one could use the model developed here to constrain ALP parameters from these observations.

To put ALP parameters, for which we expect strong mixing in HG, in context, note that there are three classes of general constraints on m and g [48]. Firm model-independent

bounds from purely laboratory experiments are weak, and the entire parameter space in Fig. 5 is allowed by them. Note, however, that the relevant range of g and m is expected to be tested by the ALPS-II experiment [99] in future. The second group consists of constraints related to production of ALPs in stellar interiors; it is more model-dependent but still considered robust. It includes direct search of solar axions with laboratory experiments on the Earth and constraints from stellar evolution. For light ALPs we discuss here, both the solar [94] and stellar [95] strongest upper limits on g coincide occasionally and do not depend on m . A large part of the (m, g) space, for which the strong mixing in HG is expected, corresponds to values of g satisfying this limit. Finally, a number of astrophysical constraints are based on the effects of ALP-photon mixing, and therefore have to assume certain magnetic fields in the sources. These constraints are more indicative than robust because cosmic magnetic fields are rarely known precisely [48]. The strongest claimed bound of this kind comes from observations of polarized magnetic white dwarfs [96]. For somewhat larger ALP masses, Ref. [100] claims a strong bound assuming the polar-cap model of pulsar emission. They are in conflict with various positive claims suggesting that ALPs with parameters disfavored by this constraint may help to solve certain discrepancies in stellar energy losses and in some gamma-ray observations of various extragalactic and Galactic objects, see e.g. reviews [2, 3, 48].

Taken at the face value in Fig. 5, this bound disfavors the parameters where the maximal mixing is most probable in HG, leaving favoured the larger- m part. However, systematic uncertainties related to the use of particular field models and to estimates of astrophysical contributions to polarization do not allow us to treat this bound as an exclusion in the particle-physics sense. Moreover, the strong mixing in HG is in fact possible for (m, g) satisfying even this bound: recall the probabilistic interpretation of Fig. 5, see Sec. 3.2. The strong mixing in HG is possible for a wide range of ALP parameters (dark shade), for both LHAASO-KM2A and Carpet-2 energies, in more than 68% of realizations of unknown parameters θ_0 and y_0 . Outside of the contours, the strong mixing is still possible for many, though less than 68% of, realizations, and it is unknown, which particular (θ_0, y_0) are realized in HG. This is illustrated in Fig. 7, where strong-mixing contours for a particular realisation of parameters discussed in Sec. 3.2 extend to higher m and lower g compared with 68% CL contours in Fig. 5.

4.3 Summary

Making use of the first Hubble Space Telescope observations of the host galaxy of GRB 221009A, we construct a toy model of its magnetic field and calculate the probability of the photon-ALP conversion there for gamma-ray energies in the LHAASO and Carpet-2 bands. Thanks to the specific edge-on orientation of the host galaxy, the conversion is strong for a large part of the ALP parameter space because of the long path of a photon in the disk magnetic field, for both bands. In the Milky Way, the GRB was also seen through the disk, which opens up the possibility of efficient photon-ALP conversion in the host galaxy and reconversion in the Milky Way. This could help to explain the detection of anomalously energetic photon-like events from the GRB, if more detailed analysis of the yet unpublished spectra would support the anomaly. If not, the conversion model presented here might be used to constrain ALP parameters.

A Expressions for the field model

This supplementary section collects explicit expressions for calculation of the magnetic field in the host galaxy of GRB 221009A within the toy model constructed in Sec. 2.2. See the main text and [61, 75] for explanations. Numerical values of parameters are collected in Table 1.

We introduce the cylindrical coordinate system (r, θ, z) with the origin in the host galaxy center. Here, r is the radial distance in the disk plane, θ is the angle in the disk plane, and z is the height above the disk plane. The angle θ_0 measures the orientation of the overall spiral structure with respect to the line $\theta = 0$; conversion probabilities in the main text were averaged over θ_0 . The disk and toroidal halo field components are set to 0 at $r^2 + z^2 > R_{\text{lim}}^2$. Dimensionful field components are denoted as (B_r, B_θ, B_z) .

A.1 Disk field

These expressions describe the disk field in the parametrization of Ref. [61]:

$$b(r) = \begin{cases} B_0 \frac{R}{R_c \cos \theta_0}, & r < R_c, \\ B_0 \frac{R}{r \cos \theta_0}, & r \geq R_c; \end{cases}$$

$$B_d(r, \theta, z) = \begin{cases} b(r) \cos \left(\theta - \frac{1}{\tan p} \ln \frac{R_{c1}}{R} + \theta_0 \right) e^{-|z|/z_0}, & r < R_{c1}, \\ b(r) \cos \left(\theta - \frac{1}{\tan p} \ln \frac{r}{R} + \theta_0 \right) e^{-|z|/z_0}, & r \geq R_{c1}. \end{cases}$$

A.2 Toroidal halo field

These expressions describe the halo field in the parametrization of Ref. [61]:

$$B_H(r, \theta, z) = \text{sign}(z) B_{0H} \left[1 + \left(\frac{|z| - z_{0H}}{z_{1H}} \right)^2 \right]^{-1} \frac{r}{R_{0H}} \exp \left(1 - \frac{r}{R_{0H}} \right),$$

where

$$z_{1H} = \begin{cases} z_{11H}, & r < R_c, \\ z_{12H}, & r \geq R_c. \end{cases}$$

A.3 X-shaped halo field

These expressions describe the additional component of the halo field from Ref. [75]:

$$r_1(r, z) = 1/(1 + az^2);$$

$$B_c(r, z) = B_1 \exp \left(-r_1(r, z) \frac{r}{L_X} \right);$$

$$B_{rX}(r, z) = 2ar_1(r, z)^3 r z B_c(r, z);$$

$$B_{zX}(r, z) = \begin{cases} r_1(R_{c1}, z)^2 B_c(R_{c1}, z), & r < R_{c1}, \\ r_1(r, z)^2 B_c(r, z), & r \geq R_{c1}. \end{cases}$$

A.4 Total field components

These are the components of the total field in our model, in cylindrical coordinates:

$$B_r(r, \theta, z) = B(r, \theta, z) \sin p + B_{rX}(r, z);$$

$$B_\theta(r, \theta, z) = B(r, \theta, z) \cos p + B_H(r, \theta, z);$$

$$B_z(r, z) = B_{zX}(r, z).$$

Parameter	Value	Parameter	Value
B_0	4.39 μG	z_0	0.49 kpc
$B_{0\text{H}}$	2.19 μG	$R_{0\text{H}}$	3.92 kpc
B_1	2.19 μG	$z_{0\text{H}}$	0.637 kpc
p	-6°	$z_{11\text{H}}$	0.1225 kpc
d	-0.294 kpc	$z_{12\text{H}}$	0.196 kpc
R	4.165 kpc	R_{c1}	1.225 kpc
R_{c}	2.94 kpc	a	0.065 kpc^{-2}
R_{lim}	9.8 kpc	L_{X}	14.7 kpc

Table 1. Parameters of the field model.

Acknowledgments

The author thanks Dmitry Gorbunov, Maxim Pshirkov, Grigory Rubtsov and Peter Tinyakov for discussions. This work is supported by the RSF grant 22-12-00253.

Note added. After the submission of the present paper, the LHAASO collaboration published a preprint [101] with some additional KM2A data, which were subsequently used by Gao et al. [102] to constrain some ALP parameters with the help of the HG magnetic-field model constructed here.

References

- [1] A. Nikishov, *Absorption of high-energy photons in the universe*, *Sov. Phys. JETP* **14** (1962) 393.
- [2] S.V. Troitsky, *Axion-like particles and the propagation of gamma rays over astronomical distances*, *JETP Lett.* **105** (2017) 55 [[1612.01864](#)].
- [3] G. Galanti and M. Roncadelli, *Axion-like Particles Implications for High-Energy Astrophysics*, *Universe* **8** (2022) 253 [[2205.00940](#)].
- [4] H. Martínez-Huerta, R.G. Lang and V. de Souza, *Lorentz Invariance Violation Tests in Astroparticle Physics*, *Symmetry* **12** (2020) 1232.
- [5] G. Raffelt and L. Stodolsky, *Mixing of the Photon with Low Mass Particles*, *Phys. Rev. D* **37** (1988) 1237.
- [6] C. Csaki, N. Kaloper, M. Peloso and J. Terning, *Super GZK photons from photon axion mixing*, *JCAP* **05** (2003) 005 [[hep-ph/0302030](#)].
- [7] A. De Angelis, M. Roncadelli and O. Mansutti, *Evidence for a new light spin-zero boson from cosmological gamma-ray propagation?*, *Phys. Rev. D* **76** (2007) 121301 [[0707.4312](#)].
- [8] M. Simet, D. Hooper and P.D. Serpico, *The Milky Way as a Kiloparsec-Scale Axionscope*, *Phys. Rev. D* **77** (2008) 063001 [[0712.2825](#)].
- [9] M. Fairbairn, T. Rashba and S.V. Troitsky, *Photon-axion mixing and ultra-high-energy cosmic rays from BL Lac type objects - Shining light through the Universe*, *Phys. Rev. D* **84** (2011) 125019 [[0901.4085](#)].
- [10] S. Troitsky, *Towards discrimination between galactic and intergalactic axion-photon mixing*, *Phys. Rev. D* **93** (2016) 045014 [[1507.08640](#)].
- [11] M.A. Williams et al., *GRB 221009A: Discovery of an Exceptionally Rare Nearby and Energetic Gamma-Ray Burst*, *Astrophys. J. Lett.* **946** (2023) L24 [[2302.03642](#)].

- [12] S. Lesage et al., *Fermi-GBM Discovery of GRB 221009A: An Extraordinarily Bright GRB from Onset to Afterglow*, *Astrophys. J. Lett.* **952** (2023) L42 [2303.14172].
- [13] A.J. Castro-Tirado et al., *GRB 221009A: 10.4m GTC spectroscopic redshift confirmation*, *GCN Circular* **32686** (2022) .
- [14] D.B. Malesani et al., *The brightest GRB ever detected: GRB 221009A as a highly luminous event at $z = 0.151$* , [2302.07891](#).
- [15] E. Burns et al., *GRB 221009A: The BOAT*, *Astrophys. J. Lett.* **946** (2023) L31 [2302.14037].
- [16] L. Lan et al., *GRB 221009A: An Ordinary Nearby GRB with Extraordinary Observational Properties*, *Astrophys. J. Lett.* **949** (2023) L4 [2303.10804].
- [17] D. Frederiks et al., *Properties of the Extremely Energetic GRB 221009A from Konus-WIND and SRG/ART-XC Observations*, *Astrophys. J. Lett.* **949** (2023) L7 [2302.13383].
- [18] R. Pillera et al., *GRB 221009A: Fermi-LAT refined analysis*, *GCN Circular* **32658** (2022) .
- [19] Z.-Q. Xia, Y. Wang, Q. Yuan and Y.-Z. Fan, *An inter-galactic magnetic field strength of $\sim 4 \times 10^{-17}$ G inferred with GRB 221009A*, [2210.13052](#).
- [20] R.-Y. Liu, H.-M. Zhang and X.-Y. Wang, *Constraints on Gamma-Ray Burst Models from GRB 221009A: GeV Gamma Rays versus High-energy Neutrinos*, *Astrophys. J. Lett.* **943** (2023) L2 [2211.14200].
- [21] T. Laskar et al., *The Radio to GeV Afterglow of GRB 221009A*, *Astrophys. J. Lett.* **946** (2023) L23 [2302.04388].
- [22] B. Stern and I. Tkachev, *GRB 221009A, its precursor and two afterglows in the Fermi data*, [2303.03855](#).
- [23] LHAASO collaboration, *A tera-electron volt afterglow from a narrow jet in an extremely bright gamma-ray burst*, *Science* **380** (2023) adg9328 [2306.06372].
- [24] Y. Huang et al., *LHAASO observed GRB 221009A with more than 5000 VHE photons up to around 18 TeV*, *GCN Circular* **32677** (2022) .
- [25] D. Dzhappuev et al., *Swift J1913.1+1946/GRB 221009A: detection of a 250-TeV photon-like air shower by Carpet-2*, *The Astronomer's Telegram* **15669** (2022) .
- [26] X.-Y. Wang, *LHAASO observations of the brightest-of-all-time GRB 221009A*, *PoS ICRC2023* (2023) 010.
- [27] G. Galanti, L. Nava, M. Roncadelli and F. Tavecchio, *Observability of the very-high-energy emission from GRB 221009A*, [2210.05659](#).
- [28] S.V. Troitsky, *Parameters of axion-like particles required to explain high-energy photons from GRB 221009A*, *Pisma Zh. Eksp. Teor. Fiz.* **116** (2022) 745 [2210.09250].
- [29] A. Baktash, D. Horns and M. Meyer, *Interpretation of multi-TeV photons from GRB221009A*, [2210.07172](#).
- [30] G. Galanti, M. Roncadelli and F. Tavecchio, *Assessment of ALP scenarios for GRB 221009A*, [2211.06935](#).
- [31] W. Lin and T.T. Yanagida, *Electroweak Axion in Light of GRB221009A*, *Chin. Phys. Lett.* **40** (2023) 069801 [2210.08841].
- [32] S. Nakagawa, F. Takahashi, M. Yamada and W. Yin, *Axion dark matter from first-order phase transition, and very high energy photons from GRB 221009A*, *Phys. Lett. B* **839** (2023) 137824 [2210.10022].
- [33] G. Zhang and B.-Q. Ma, *Axion-Photon Conversion of LHAASO Multi-TeV and PeV Photons*, *Chin. Phys. Lett.* **40** (2023) 011401 [2210.13120].

- [34] P. Carena and M.C.D. Marsh, *On ALP scenarios and GRB 221009A*, [2211.02010](#).
- [35] L. Wang and B.-Q. Ma, *Axion-photon conversion of GRB221009A*, *Phys. Rev. D* **108** (2023) 023002 [[2304.01819](#)].
- [36] D.A. Rojas, S. Hernández-Cadena, M.M. González, A. Pratts, R. Alfaro and J. Serna-Franco, *GRB 221009A: Spectral signatures based on ALPs candidates*, [2305.05145](#).
- [37] K. Cheung, *The Role of a Heavy Neutrino in the Gamma-Ray Burst GRB-221009A*, [2210.14178](#).
- [38] A.Y. Smirnov and A. Trautner, *GRB 221009A Gamma Rays from the Radiative Decay of Heavy Neutrinos?*, *Phys. Rev. Lett.* **131** (2023) 021002 [[2211.00634](#)].
- [39] V. Brdar and Y.-Y. Li, *Neutrino origin of LHAASO's 18 TeV GRB221009A photon*, *Phys. Lett. B* **839** (2023) 137763 [[2211.02028](#)].
- [40] J. Huang, Y. Wang, B. Yu and S. Zhou, *Invisible neutrino decays as origin of TeV gamma rays from GRB221009A*, *JCAP* **04** (2023) 056 [[2212.03477](#)].
- [41] S. Balaji, M.E. Ramirez-Quezada, J. Silk and Y. Zhang, *Light scalar explanation for the 18 TeV GRB 221009A*, *Phys. Rev. D* **107** (2023) 083038 [[2301.02258](#)].
- [42] J. Zhu and B.-Q. Ma, *Light speed variation from GRB 221009A*, *J. Phys. G* **50** (2023) 06LT01 [[2210.11376](#)].
- [43] J.D. Finke and S. Razzaque, *Possible Evidence for Lorentz Invariance Violation in Gamma-Ray Burst 221009A*, *Astrophys. J. Lett.* **942** (2023) L21 [[2210.11261](#)].
- [44] H. Li and B.-Q. Ma, *Lorentz invariance violation induced threshold anomaly versus very-high energy cosmic photon emission from GRB 221009A*, *Astropart. Phys.* **148** (2023) 102831 [[2210.06338](#)].
- [45] S.-Y. Guo, M. Khlopov, L. Wu and B. Zhu, *Can sterile neutrinos explain the very high energy photons from GRB221009A?*, *Phys. Rev. D* **108** (2023) L021302 [[2301.03523](#)].
- [46] H. Li and B.-Q. Ma, *Revisiting Lorentz invariance violation from GRB 221009A*, [2306.02962](#).
- [47] M. Libanov and S. Troitsky, *On the impact of magnetic-field models in galaxy clusters on constraints on axion-like particles from the lack of irregularities in high-energy spectra of astrophysical sources*, *Phys. Lett. B* **802** (2020) 135252 [[1908.03084](#)].
- [48] PARTICLE DATA GROUP collaboration, *Review of Particle Physics*, *PTEP* **2022** (2022) 083C01.
- [49] PLANCK collaboration, *Planck intermediate results.: XLII. Large-scale Galactic magnetic fields*, *Astron. Astrophys.* **596** (2016) A103 [[1601.00546](#)].
- [50] G. Magkos and V. Pavlidou, *Deflections of ultra-high energy cosmic rays by the Milky Way magnetic field: how well can they be corrected?*, *JCAP* **02** (2019) 004 [[1802.03409](#)].
- [51] M. Unger and G. Farrar, *Progress in the Global Modeling of the Galactic Magnetic Field*, vol. 210, p. 04005, 2019, DOI [[1901.04720](#)].
- [52] M. Unger and G. Farrar, *Progress in the Global Modeling of the Galactic Magnetic Field*, *EPJ Web Conf.* **210** (2019) 04005 [[1901.04720](#)].
- [53] A.J. Levan et al., *The First JWST Spectrum of a GRB Afterglow: No Bright Supernova in Observations of the Brightest GRB of all Time, GRB 221009A*, *Astrophys. J. Lett.* **946** (2023) L28 [[2302.07761](#)].
- [54] A. de Ugarte Postigo et al., *GRB 221009A: Redshift from X-shooter/VLT*, *GCN Circular* **32648** (2022) .
- [55] L. Izzo et al., *GRB 221009A: VLT spectroscopic detection of the host galaxy*, *GCN Circular* **32765** (2022) .

- [56] T.H. Jarrett, T. Chester, R. Cutri, S.E. Schneider and J.P. Huchra, *The 2MASS Large Galaxy Atlas*, *Astron. J.* **125** (2003) 525.
- [57] P. Schmidt, M. Krause et al., *CHANG-ES. XVI. An in-depth view of the cosmic-ray transport in the edge-on spiral galaxies NGC 891 and NGC 4565*, *Astron. Astrophys.* **632** (2019) A12 [[1907.03789](#)].
- [58] I.G. Momcheva et al., *The 3D-HST Survey: Hubble Space Telescope WFC3/G141 Grism Spectra, Redshifts, and Emission Line Measurements for $\sim 100,000$ Galaxies*, *Astrophys. J. Suppl.* **225** (2016) 27 [[1510.02106](#)].
- [59] J.D. Lyman et al., *The host galaxies and explosion sites of long-duration gamma ray bursts: Hubble Space Telescope near-infrared imaging*, *Mon. Not. Roy. Astron. Soc.* **467** (2017) 1795 [[1701.05925](#)].
- [60] R. Beck, *Magnetic fields in spiral galaxies*, *Astron. Astrophys. Rev.* **24** (2015) 4 [[1509.04522](#)].
- [61] M.S. Pshirkov, P.G. Tinyakov, P.P. Kronberg and K.J. Newton-McGee, *Deriving global structure of the Galactic Magnetic Field from Faraday Rotation Measures of extragalactic sources*, *Astrophys. J.* **738** (2011) 192 [[1103.0814](#)].
- [62] R. Jansson and G.R. Farrar, *A New Model of the Galactic Magnetic Field*, *Astrophys. J.* **757** (2012) 14 [[1204.3662](#)].
- [63] V.V. Bobylev and A.T. Bajkova, *Estimation of the Radial Scale Length and Vertical Scale Height of the Galactic Thin Disk from Cepheids*, *Astronomy Letters* **47** (2021) 534 [[2110.11203](#)].
- [64] B. Schneider, E. Le Floch, M. Arabsalmani, S.D. Vergani and J.T. Palmerio, *Are the host galaxies of Long Gamma-Ray Bursts more compact than star-forming galaxies of the field?*, *Astron. Astrophys.* **666** (2022) A14 [[2206.14873](#)].
- [65] P.C. van der Kruit, *A comparison of our galaxy to NGC 891 and NGC 4565 and the structure of their spheroids.*, *Astron. Astrophys.* **140** (1984) 470.
- [66] N.Z. Scoville, D. Thakkar, J.E. Carlstrom and A.I. Sargent, *The Scale Height and Radial Distribution of Molecular Gas in NGC 891*, *Astrophys. J. Lett.* **404** (1993) L59.
- [67] M. Krause, *Magnetic fields and star formation as seen in edge-on galaxies*, in *Magnetic Fields in the Universe III - From Laboratory and Stars to Primordial Structures*, p. 155, Jan., 2012, DOI [[1111.7081](#)].
- [68] T. Wiegert et al., *CHANG-ES. IV. Radio Continuum Emission of 35 Edge-on Galaxies Observed with the Karl G. Jansky Very Large Array in D Configuration—Data Release 1*, *Astron. J.* **150** (2015) 81 [[1508.05153](#)].
- [69] S. Sukumar and R.J. Allen, *Polarized Radio Emission from the Edge-on Spiral Galaxies NGC 891 and NGC 4565*, *Astrophys. J.* **382** (1991) 100.
- [70] M. Dumke, M. Krause, R. Wielebinski and U. Klein, *Polarized radio emission at 2.8cm from a selected sample of edge-on galaxies.*, *Astron. Astrophys.* **302** (1995) 691.
- [71] M. Krause, *Magnetic Fields and Star Formation in Spiral Galaxies*, in *Revista Mexicana de Astronomia y Astrofisica Conference Series*, vol. 36 of *Revista Mexicana de Astronomia y Astrofisica Conference Series*, pp. 25–29, Aug., 2009, DOI [[0806.2060](#)].
- [72] D.D. Mulcahy et al., *Investigation of the cosmic ray population and magnetic field strength in the halo of NGC 891*, *Astron. Astrophys.* **615** (2018) A98 [[1804.00752](#)].
- [73] T.J. Jones et al., *HAWC+ Far-infrared Observations of the Magnetic Field Geometry in M51 and NGC 891*, *Astron. J.* **160** (2020) 167 [[2008.07897](#)].
- [74] M. Krause et al., *CHANG-ES. XXII. Coherent magnetic fields in the halos of spiral galaxies*, *Astron. Astrophys.* **639** (2020) A112 [[2004.14383](#)].

- [75] K. Ferrière and P. Terral, *Analytical models of X-shape magnetic fields in galactic halos*, *Astron. Astrophys.* **561** (2014) A100 [[1312.1974](#)].
- [76] S. Niklas and R. Beck, *A new approach to the radio-far infrared correlation for non-calorimeter galaxies.*, *Astron. Astrophys.* **320** (1997) 54.
- [77] D.R.G. Schleicher and R. Beck, *A new interpretation of the far-infrared - radio correlation and the expected breakdown at high redshift*, *Astron. Astrophys.* **556** (2013) A142 [[1306.6652](#)].
- [78] C. Pfrommer, M. Werhahn, R. Pakmor, P. Girichidis and C.M. Simpson, *Simulating radio synchrotron emission in star-forming galaxies: small-scale magnetic dynamo and the origin of the far-infrared–radio correlation*, *Mon. Not. Roy. Astron. Soc.* **515** (2022) 4229 [[2105.12132](#)].
- [79] V. Heesen et al., *Nearby galaxies in the LOFAR Two-metre Sky Survey. I. Insights into the non-linearity of the radio-SFR relation*, *Astron. Astrophys.* **664** (2022) A83 [[2204.00635](#)].
- [80] K.T. Chyży, S.S. Sridhar and W. Jurusik, *What drives galactic magnetism?*, *Astron. Astrophys.* **603** (2017) A121 [[1705.07187](#)].
- [81] S. Manna and S. Roy, *Magnetic Fields, Star Formation Rates, and Gas Densities at Sub-kiloparsec Scales in a Pilot Sample of Nearby Galaxies*, *Astrophys. J.* **944** (2023) 86 [[2301.03752](#)].
- [82] T.A. Thompson, E. Quataert, E. Waxman, N. Murray and C.L. Martin, *Magnetic fields in starburst galaxies and the origin of the fir-radio correlation*, *Astrophys. J.* **645** (2006) 186 [[astro-ph/0601626](#)].
- [83] R.J.J. Grand, F.A. Gómez et al., *The Auriga Project: the properties and formation mechanisms of disc galaxies across cosmic time*, *Mon. Not. Roy. Astron. Soc.* **467** (2017) 179 [[1610.01159](#)].
- [84] R. Pakmor et al., *Magnetic field formation in the Milky Way like disc galaxies of the Auriga project*, *Mon. Not. Roy. Astron. Soc.* **469** (2017) 3185 [[1701.07028](#)].
- [85] P. Popesso, A. Concas, G. Cresci, S. Belli, G. Rodighiero, H. Inami et al., *The Main Sequence of star-forming galaxies across cosmic times*, *Mon. Not. Roy. Astron. Soc.* **519** (2023) 1526 [[2203.10487](#)].
- [86] E.M. Xilouris et al., *Optical and NIR modelling of NGC 891*, *Astron. Astrophys.* **331** (1998) 894.
- [87] L. Maiani, R. Petronzio and E. Zavattini, *Effects of Nearly Massless, Spin Zero Particles on Light Propagation in a Magnetic Field*, *Phys. Lett. B* **175** (1986) 359.
- [88] A. Dobrynina, A. Kartavtsev and G. Raffelt, *Photon-photon dispersion of TeV gamma rays and its role for photon-ALP conversion*, *Phys. Rev. D* **91** (2015) 083003 [[1412.4777](#)].
- [89] M. Kachelriess and J. Tjemsland, *On the origin and the detection of characteristic axion wiggles in photon spectra*, *JCAP* **01** (2022) 025 [[2111.08303](#)].
- [90] S.L. Adler, *Photon splitting and photon dispersion in a strong magnetic field*, *Annals Phys.* **67** (1971) 599.
- [91] V.I. Ritus, *Radiative effects and their amplification in an intense electromagnetic field.*, *Proc. Lebedev Phys. Inst. Acad. Sci. USSR* **168** (1987) 180.
- [92] L. Ciotti, *Stellar systems following the $R1/m$ luminosity law.*, *Astron. Astrophys.* **249** (1991) 99.
- [93] A.W. Graham and S.P. Driver, *A Concise reference to (projected) Sersic $R^{**1/n}$ quantities, including concentration, profile slopes, Petrosian indices, and Kron magnitudes*, *Publ. Astron. Soc. Austral.* **22** (2005) 118 [[astro-ph/0503176](#)].
- [94] CAST collaboration, *New CAST Limit on the Axion-Photon Interaction*, *Nature Phys.* **13** (2017) 584 [[1705.02290](#)].

- [95] A. Ayala, I. Domínguez, M. Giannotti, A. Mirizzi and O. Straniero, *Revisiting the bound on axion-photon coupling from Globular Clusters*, *Phys. Rev. Lett.* **113** (2014) 191302 [[1406.6053](#)].
- [96] C. Dessert, D. Dunskey and B.R. Safdi, *Upper limit on the axion-photon coupling from magnetic white dwarf polarization*, *Phys. Rev. D* **105** (2022) 103034 [[2203.04319](#)].
- [97] K. Pattle, L. Fissel, M. Tahani, T. Liu and E. Ntormousi, *Magnetic fields in star formation: from clouds to cores*, [2203.11179](#).
- [98] P. Carena, C. Evoli, M. Giannotti, A. Mirizzi and D. Montanino, *Turbulent axion-photon conversions in the Milky Way*, *Phys. Rev. D* **104** (2021) 023003 [[2104.13935](#)].
- [99] R. Bähre et al., *Any light particle search II — Technical Design Report*, *JINST* **8** (2013) T09001 [[1302.5647](#)].
- [100] D. Noordhuis, A. Prabhu, S.J. Witte, A.Y. Chen, F. Cruz and C. Weniger, *Novel Constraints on Axions Produced in Pulsar Polar-Cap Cascades*, *Phys. Rev. Lett.* **131** (2023) 111004 [[2209.09917](#)].
- [101] LHAASO collaboration, *Very high energy gamma-ray emission beyond 10 TeV from GRB 221009A*, [2310.08845](#).
- [102] L.-Q. Gao, X.-J. Bi, J. Li, R.-M. Yao and P.-F. Yin, *Constraints on Axion-like Particles from the Observation of GRB 221009A by LHAASO*, [2310.11391](#).